NANOMATERIALS AND NANOTECHNOLOGY

Nanomaterials and Nanotechnology
Volume 10: 1–10

DOI: 10.1177/1847980420949349
journals.sagepub.com/home/nax
SAGE

Substitutional impurities in monolayer hexagonal boron nitride as single-photon emitters

Michele Re Fiorentin[1], Kiptiemoi Korir Kiprono[2], and Francesca Risplendi[3]

Abstract

Single-photon emitters in hexagonal boron nitride have attracted great attention over the last few years due to their excellent optoelectronical properties. Despite the vast range of results reported in the literature, studies on substitutional impurities belonging to the 13th and 15th groups have not been reported yet. Here, through theoretical modeling, we provide direct evidence that hexagonal boron nitride can be opportunely modified by introducing impurity atoms such as aluminum or phosphorus that may work as color centers for single-photon emission. By means of density functional theory, we focus on determining the structural stability, induced strain, and charge states of such defects and discuss their electronic properties. Nitrogen substitutions with heteroatoms of group 15 are shown to provide attractive features (e.g. deep defect levels and localized defect states) for single-photon emission. These results may open up new possibilities for employing innovative quantum emitters based on hexagonal boron nitride for emerging applications in nanophotonics and nanoscale sensing devices.

Keywords

Boron nitride, single-photon emitter, substitutional impurity

Date received: 30 April 2020; accepted: 4 July 2020

Topic: Polymer Nanocomposites and Nanostructured Materials
Topic Editor: Fabrizio Cleri
Associate Editor: Luca Camilli

Introduction

The importance of photonic technologies is steadily growing in our daily lives. In the past few decades, developments in light generation and manipulation have allowed for the widespread diffusion of efficient devices, such as lasers and light-emitting diodes. Today, stimulated by the wide field of possible applications, research is focusing on the realization and development of new light sources, able to produce photons whose statistics and correlations are eminently quantum-mechanical. Such nonclassical light sources rely on a fundamental component: the single-photon emitter (SPE). The ideal SPE is an on demand, deterministic source delivering light pulses in a well-defined polarization and spatiotemporal mode and containing exactly one photon. Unlike classical light sources, SPEs are fundamental quantum devices for many scalable and leading technologies, such as quantum information,[1] quantum computing and simulation,[2] precision metrology and imaging,[3] and quantum communication.[4]

[1] Center for Sustainable Future Technologies, Istituto Italiano di Tecnologia, Torino, Italy
[2] Physics Department, Moi University, Eldoret, Kenya
[3] Dipartimento di Scienza Applicata e Tecnologia, Politecnico di Torino, Torino, Italy

Corresponding authors:
Michele Re Fiorentin, Center for Sustainable Future Technologies, Istituto Italiano di Tecnologia, via Livorno 60, 10144 Torino, Italy.
Email: michele.refiorentin@iit.it

Francesca Risplendi, Dipartimento di Scienza Applicata e Tecnologia, Politecnico di Torino, corso Duca degli Abruzzi 24, 10129 Torino, Italy.
Email: francesca.risplendi@polito.it

Up to now, single-photon sources obtained by means of isolated color centers in wide bandgap semiconductors have been realized in a number of systems as three-dimensional (3D) materials, such as diamond[5–7] and gallium nitride,[7,8] 2D materials such as hexagonal boron nitride (h-BN),[9] one-dimensional materials, such as carbon nanotubes[6] and indium phosphide nanowires,[10] and zero-dimensional materials, such as gallium arsenide (GaAs) and indium gallium arsenide quantum dots.[11,12] The ability to tailor and control quantum emitters, to realize efficient and scalable architectures, depends on site-selective defect engineering. To avoid recombination due to thermal effects, defect energy levels need to be deep in the semiconductor bandgap. At the same time, defect states should not present strong hybridization with the host matrix, so that the relative energy levels show little dispersion in reciprocal space and allow for the emission of photons with definite wavelength.[13] Additionally, without taking into account the drawbacks that limit their applications such as, for example, low temperature functionality and low brightness, one of the major challenges is that point defects need to be precisely positioned. This is particularly difficult for conventional 3D semiconductors, where defects are often buried deep within the bulk structure as, for example, the nitrogen vacancy center in diamond.[14] One route to overcome this problem is to reduce the dimensionality of the material.

Over the last decade, it has become possible to fabricate and manipulate atomically thin materials that show intriguing electronic and optical properties. In addition, the 2D geometry of SPEs confined to a single-layer material can greatly enhance the photon extraction efficiency, potentially allowing for simplified integration in photonic circuits. Among them, h-BN has attracted great attention due to its high chemical and thermal stability[15,16] and has been commonly employed both as substrate and active material in several electronic devices.[17–19] It has also shown a low dielectric constant and high thermal conductivity besides a wide electronic bandgap, a fundamental requirement for being employed, upon opportune engineerization, as SPE.[20,21] Recently, ultrabright, polarized, and stable at room temperature single-photon emission in h-BN associated with deep energy level defect states within the large bandgap has been reported.[22–31] Several experimental works provide evidence that the emission may be associated with B or N vacancies,[28,31] a carbon[28,32–34] or oxygen[31,35] substitutional impurity at nitrogen site, and carbon substituting at B site.[31] All of these results indicate that h-BN should be one of the promising host materials to achieve full spectral range from ultraviolet to near-infrared single-photon source. However, to the best of our knowledge, substitutional impurities belonging to group 13 (icosagens[36]) or group 15 (pnictogens) in h-BN have not been reported yet.

Here we focus on substitutional impurities in h-BN, in which a single atom of group 13 substitutes one B atom or a single atom of group 15 substitutes one N atom in the pristine monolayer, and perform a consistent theoretical analysis of these different substitutional defects by means of *ab initio* techniques based on density functional theory (DFT). In particular, for each of the substitutions, we compute the formation energies at different charge states and compare the corresponding electronic structures. We also discuss the obtained electronic properties in terms of the defect induced strain. Our results demonstrate that the inclusion of group 15 atoms in the h-BN matrix gives rise to defect states that meet fundamental requirements of single-photon emission, presenting deep energy levels within the h-BN bandgap and strong spatial localization.

This work will help open up possibilities for employing quantum emitters in 2D materials for emerging applications in nanophotonics and nanoscale sensing devices. The successful computational discovery of new color centers in h-BN will bring about new scientific insights regarding the ultimate potential of nanophotonics and nanoscale devices. Furthermore, all the results obtained in this project can also be used in designing a number of other optoelectronic devices such as lasers and waveguides, to achieve a larger efficiency compared to currently used technologies.

Computational details

All theoretical calculations are based on spin-polarized DFT as implemented in the Quantum ESPRESSO package (version 6.4.1).[37,38] The Kohn–Sham equations are solved using norm conserving pseudopotentials to describe the electron–ion interaction,[39] employing the gradient corrected Perdew–Burke–Ernzerhof (PBE) functional[40] to describe the exchange–correlation effects, and expanding the electronic wave functions in plane waves (PW). For all calculations, we adopt a PW energy cutoff of 80 Ry. $n \times n$ h-BN supercells, with n varying from 4 to 8, are employed to investigate the substitutional impurities. A vacuum of at least 10 Å thickness is added in the direction perpendicular to the 2D layers to avoid spurious interaction between periodic replicas. The Brillouin zone of the primitive cell is sampled employing a $12 \times 12 \times 1$ Monkhorst–Pack mesh.[41] All structures are relaxed by minimizing the atomic forces; convergence is assumed when the maximum component of the residual forces on the ions was smaller than 10^{-4} Ry/Bohr.

The formation energy of a defect in h-BN with zero charge in the cell (neutral defect) can be written as[42,43]

$$E^f[X^0] = E_{\text{tot}}[X^0] - E^p_{\text{tot}} - n_{\text{B}}\mu_{\text{B}} - n_{\text{N}}\mu_{\text{N}} - \sum_X n_X\mu_X \tag{1}$$

where $E_{\text{tot}}[X^0]$ is the total energy of the defected layer, E^p_{tot} is the total energy of the pristine layer, n_{N} and n_{B} are, respectively, the number of N and B atoms added to

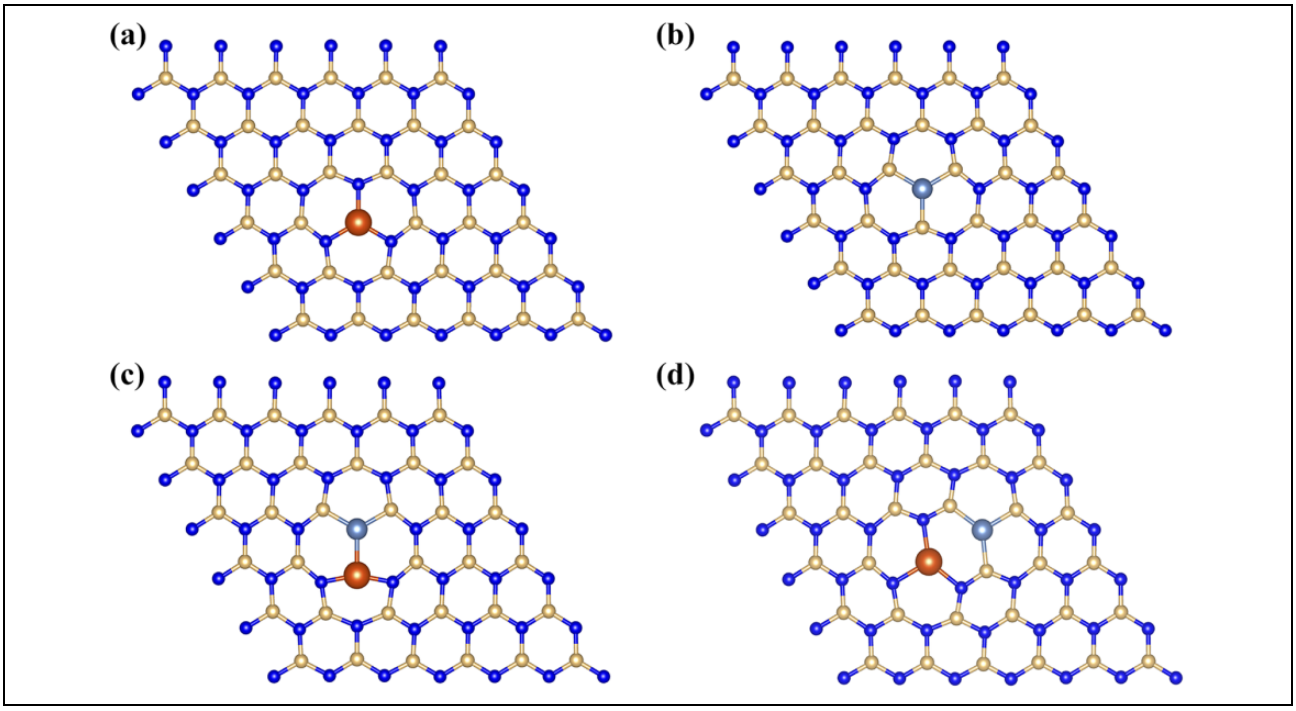

Figure 1. Ball-and-stick representation of optimized geometries of substitutional defect in h-BN. Nitrogen and boron atoms are represented by blue and yellow spheres, respectively. (a) Single substitution of a B atom by a group 13 heteroatom (orange sphere). (b) Single substitution of an N atom by a group 15 heteroatom (gray sphere). (c) and (d) Joint substitutions of a B atom and an N atom in two different geometries. h-BN: hexagonal boron nitride.

(positive) or removed from (negative) the pristine layer, and n_X is the number of atoms of species X added to the system. The chemical potential of N (B) can be expressed as $\mu_{\mathrm{N(B)}} = \mu^0_{\mathrm{N(B)}} + \Delta\mu_{\mathrm{N(B)}}$, where the reference potential μ^0_{N} is taken as half the energy of an N_2 molecule at standard conditions and μ^0_{B} as the energy of a boron atom in the rhombohedral bulk structure with $R\bar{3}m$ symmetry. The chemical potentials of the heteroatoms X are taken as the energies of a single atom in the relative bulk structure stable at room temperature. The definitions of the chemical potentials imply $\mu_{\mathrm{N}} \leq \mu^0_{\mathrm{N}}$ and $\mu_{\mathrm{B}} \leq \mu^0_{\mathrm{B}}$, and thermodynamical equilibrium requires $\mu_{\mathrm{h-BN}} = \mu_{\mathrm{N}} + \mu_{\mathrm{B}}$, where $\mu_{\mathrm{h-BN}}$ is taken as the energy of one formula unit of monolayer h-BN. By defining[44] $\Delta\mu = \Delta\mu_{\mathrm{B}} - \Delta\mu_{\mathrm{N}}$ and using the equilibrium relation between chemical potentials, it is possible to rewrite equation (1) as

$$E^f[X^0] = E^{'}_{\mathrm{tot}}[X^0] - \frac{1}{2}(n_{\mathrm{B}} - n_{\mathrm{N}})\Delta\mu - \sum_X n_X\mu_X \qquad (2)$$

where $E^{'}_{\mathrm{tot}}[X^0] = E_{\mathrm{tot}}[X^0] - E^p_{\mathrm{tot}} + 1/2(n_{\mathrm{B}} - n_{\mathrm{N}})(\mu^0_{\mathrm{N}} - \mu^0_{\mathrm{B}}) - 1/2(n_{\mathrm{N}} + n_{\mathrm{B}})\mu_{\mathrm{h-BN}}$. This allows to impose meaningful constraints on the $\Delta\mu$ parameter by introducing the enthalpy of formation of an h-BN layer $\Delta H^f_{\mathrm{h-BN}} = \mu_{\mathrm{h-BN}} - \mu^0_{\mathrm{B}} - \mu^0_{\mathrm{N}}$, so that

$$\Delta H^f_{\mathrm{h-BN}} \leq \Delta\mu \leq -\Delta H^f_{\mathrm{h-BN}} \qquad (3)$$

The formation energy of a charged defect X^q is obtained as[45]

$$E^f[X^q] = E^{'}_{\mathrm{tot}}[X^q] - \frac{1}{2}(n_{\mathrm{B}} - n_{\mathrm{N}})\Delta\mu - \sum_X n_X\mu_X + q(\varepsilon_{\mathrm{F}} + E_{\mathrm{VBM}}) \qquad (4)$$

where q is the total charge, E_{VBM} is the valence band maximum (VBM) energy of pristine h-BN with respect to the vacuum and ε_{F} is the Fermi level with respect to VBM. We obtain $E^f[X^q]$ by computing the formation energy in supercells with increasing size and extrapolating its value to the infinite volume limit. A converged result is recovered if all three dimensions are uniformly scaled, thus avoiding the inclusion of correction terms[46–48] in equation (4). Once the formation energies for a defect with different charges q_1 and q_2 are known, it is possible to obtain the charge-state transition level as

$$\varepsilon(q_1/q_2) = \frac{E^f[X^{q_1}, \varepsilon_{\mathrm{F}} = 0] - E^f[X^{q_2}, \varepsilon_{\mathrm{F}} = 0]}{q_2 - q_1} \qquad (5)$$

so that for $\varepsilon_{\mathrm{F}} < \varepsilon(q_1/q_2)$ the defect is stable in the charge state q_1, while for $\varepsilon_{\mathrm{F}} > \varepsilon(q_1/q_2)$ it is stable in the charge state q_2.

Results and discussion

Structural properties

In Figure 1, we show the representative geometries of the classes of substitutional defects analyzed in this work: (a)

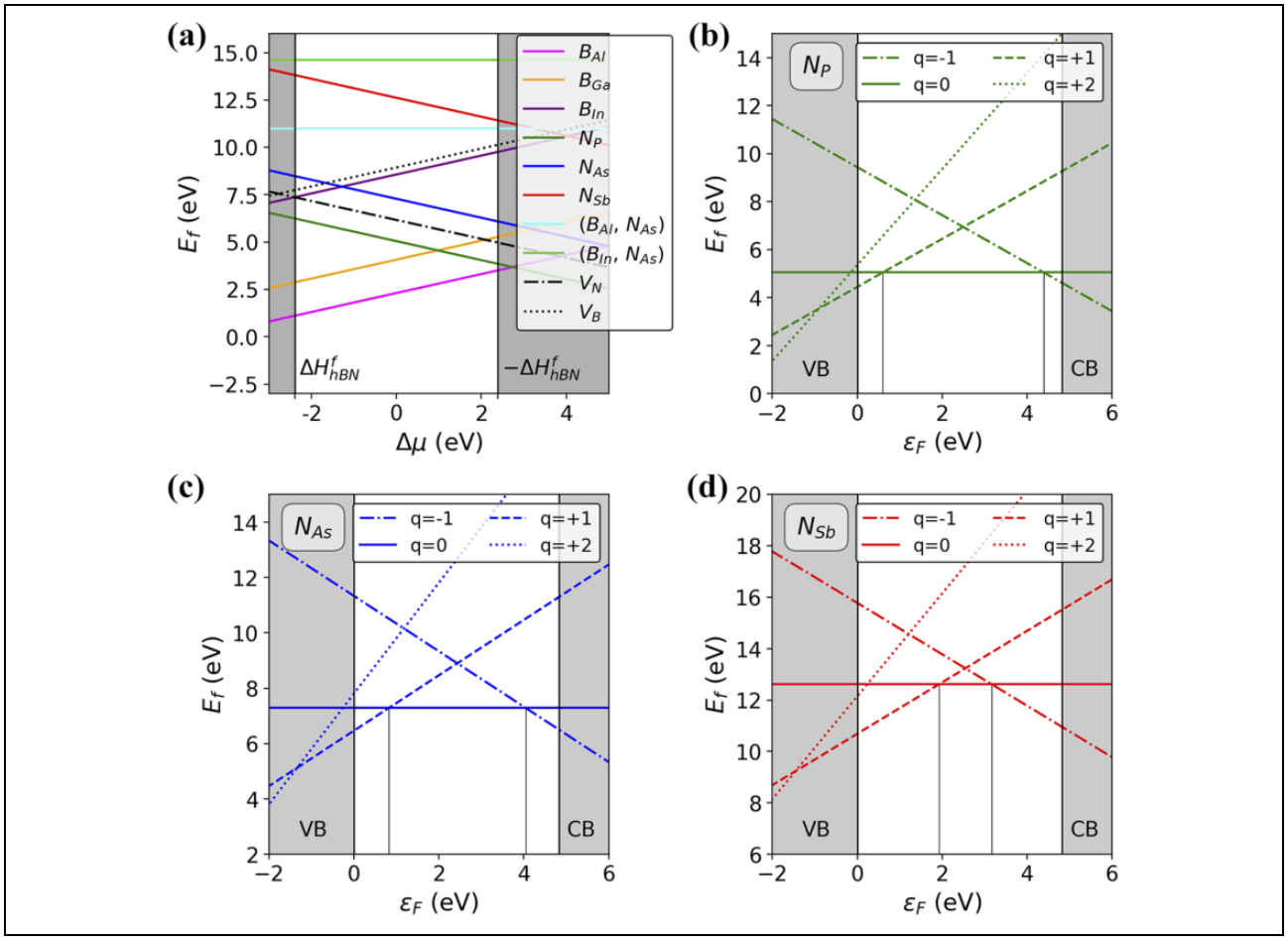

Figure 2. Formation energies of substitutional defects in h-BN. (a) Formation energies of substitutional defects as a function of $\Delta\mu$, equation (2). Double substitutions (B_{Al}, N_{As}) and (B_{In}, N_{As}) are drawn in solid cyan and green lines, respectively. Single boron and nitrogen vacancies in h-BN are shown in dotted and dash-dotted black lines, respectively. The shaded areas mark the excluded regions according to equation (3). (b), (c), and (d) Formation energy versus Fermi level of different charge states for the N_P, N_{As}, and N_{Sb}, respectively, equation (1). The vertical thin lines mark the charge-state transition levels, equation (5), while the shaded areas represent the VB and CB of pristine h-BN. h-BN: hexagonal boron nitride; VB: valence band; CB: conduction band.

single substitution of a boron atom with a group 13 heteroatom (Al, Ga, In), (b) single substitution of a nitrogen atom with a group 15 heteroatom (P, As, Sb), (c) joint substitution of two adjacent boron and nitrogen atoms, (d) joint substitution of two nonadjacent boron and nitrogen atoms. We also investigated the case of triple substitutions; however, such cases will not be discussed here due to their excessively high formation energy.

In Figure 2(a), we report the formation energies of neutral substitutional defects as computed with equation (2). In particular, we show the dependence on $\Delta\mu$ in the case of a single boron atom substituted by Al, Ga, In (B_{Al}, B_{Ga}, B_{In}) and of a single nitrogen atom replaced by P, As, and Sb (N_P, N_{As}, N_{Sb}). Since $\Delta\mu > 0$ ($\Delta\mu < 0$) corresponds to boron-rich/nitrogen-lean (boron-lean/nitrogen-rich) conditions, B-substitutions have positive slopes, while N-substitutions display the opposite behavior. In our setup, double substitutions, such as (B_{Al}, N_{As}) (solid black line) and (B_{In}, N_{As}) (dashed black line), are constant with respect to $\Delta\mu$. No substitutional defect has a negative formation energy and the most thermodynamically favored appears to be B_{Al} throughout the whole variability range of $\Delta\mu$. We notice that, in general, the formation energy increases moving down along the group of the heteroatoms, so that $E^f[B_{Al}] < E^f[B_{Ga}] < E^f[B_{In}]$ and likewise $E^f[N_P] < E^f[N_{As}] < E^f[N_{Sb}]$. Furthermore, $E^f[(B_{Al}, N_{As})] < E^f[(B_{In}, N_{As})]$. In Figure 2(a), we also report the formation energy of a single boron (nitrogen) atom vacancy V_B (V_N), which is in excellent agreement with previous calculations.[49]

The hierarchies in defect formation energies are reflected by the amount of strain introduced in the h-BN lattice by the introduced heteroatom. In Figure 3, we schematically report the optimized geometries of the studied substitutional defects highlighting in color the percentage difference of each bond length with respect to the equilibrium bond length of pristine h-BN. This way, compressed bonds appear in shades of blue, ranging from 0% to −5%

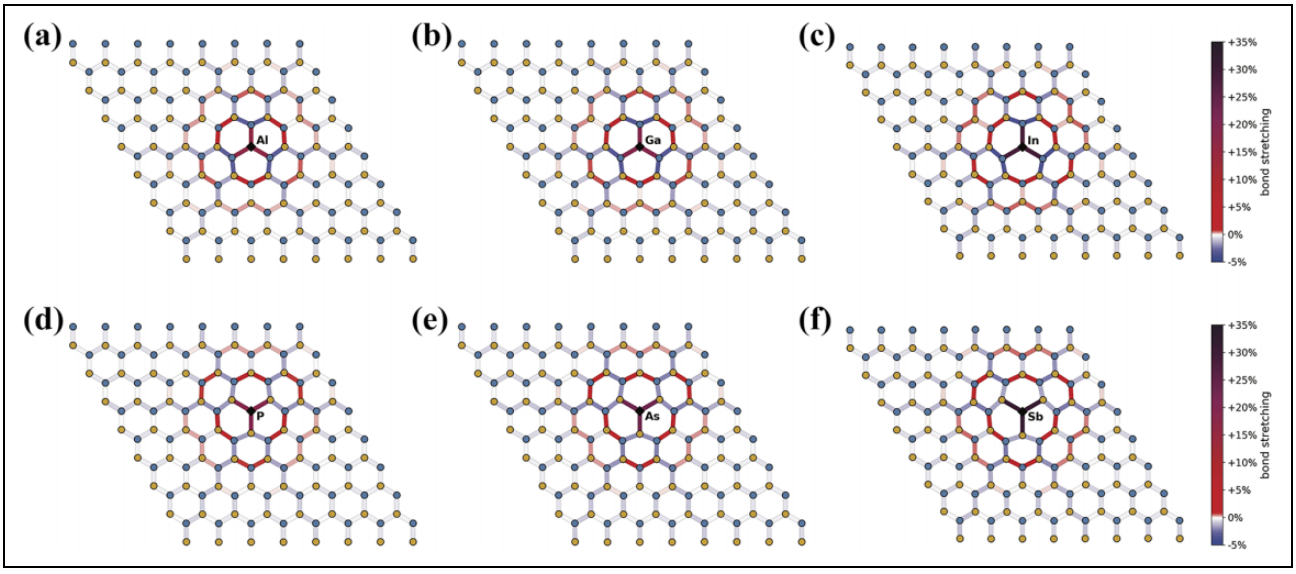

Figure 3. Representation of bond stretching and compression for the analyzed point defects. Bonds between atoms are color-coded according to their percentage difference from the equilibrium B–N bond in h-BN. Compression values range from 0% to −5% and are colored with blue shades, elongation values range from 0% to +35% and are colored in red–purple shades. Boron and nitrogen atoms are represented by blue and orange dots, respectively. The heteroatoms are marked by black diamonds and labeled. h-BN: hexagonal boron nitride.

compression, while elongated bonds are colored in shades of red–purple, from 0% to +5% (light red) to +35% (dark purple) stretching. It is possible to notice that the most distorted bonds directly involve the heteroatom and show a significant stretching. For B-substitutions, we have +17% for N–Al bonds in B_{Al} (panel a), +19% for N–Ga bonds in B_{Ga} (panel b), and +29% for N–In bonds in B_{In} (panel c), in agreement with the increasing atomic radius of Al, Ga, and In. Similarly, for N-substitutions, we found +19% for B–P bonds in N_P (panel d), +23% for B–As bonds in N_{As} (panel e), and +31% for B–Sb bonds in N_{Sb} (panel f), again in agreement with the atomic radius trends. The variations among B–N bonds in the lattice never exceed ±5%.

For the single-substitution defects, we explored the stability of different charge states which can originate interesting features in the electronic band structure and, consequently, on the emission spectrum (see next subsection). In Figure 2, we show the dependence on the Fermi level ε_F of the formation energy of N_P (panel b), N_{As} (panel c), and N_{Sb} (panel (d)), in different charge states. For these calculations, the chemical potentials of N and B atoms are such that $\Delta\mu = 0$.

For each substitutional defect, we investigate the charge states $q = -1, 0, +1, +2$ and report the relative transition levels in Table 1. Charge state +2 is never found to be favored for values of the Fermi level within the electronic gap of pristine h-BN. The stability ranges of charge states −1 and +1 become larger while moving from P to Sb. In Table 1, we also show the calculated ionization potential $IP = E_{tot}[X^{+1}] - E_{tot}[X^0]$ and electron affinity $EA = E_{tot}[X^0] - E_{tot}[X^{-1}]$ for the nitrogen substitutional defects.

Table 1. Charge-state transition levels (equation (4)), ionization potential ($IP = E_{tot}[X^{+1}] - E_{tot}[X^0]$) and electron affinity ($EA = E_{tot}[X^0] - E_{tot}[X^{-1}]$) for the analyzed substitutions of a single nitrogen atom.[a]

	N_P	N_{As}	N_{Sb}
$\varepsilon(-1/0)$ (eV)	4.39	4.05	3.16
$\varepsilon(0/1)$ (eV)	0.60	0.82	1.93
$\varepsilon(1/2)$ (eV)	−0.91	−1.34	−1.45
IP (eV)	3.30	2.94	2.35
EA (eV)	−1.08	−1.11	−1.14

h-BN: hexagonal boron nitride; IP: ionization potential; EA: electron affinity.
[a]The values of $\varepsilon(q_1/q_2)$ are referred to the top of the valence band of pristine h-BN.

Electronic properties

To rationalize the behavior of substitutional impurities, the different alignment of the defect states with respect to the h-BN bands has to be taken into account. With this aim, the electronic properties of different systems are analyzed in terms of density of states and projected density of states. The h-BN upper valence band (VB) has predominantly N-2p character with some hybridization with B-2p orbitals, while the lower conduction band (CB) has mainly B-2p character. Upon N-substitutional impurity inclusions, occupied defect states attributed to the p orbitals of P, As, or Sb appear in the h-BN bandgap located at more than +1 eV from VBM, as reported in Figure 4 (panels (d), (e), and (f)). In B-substitutional impurity inclusions, Figure 4(a), (b), and (c), only in B_{Al} and B_{In} cases, an unoccupied defect

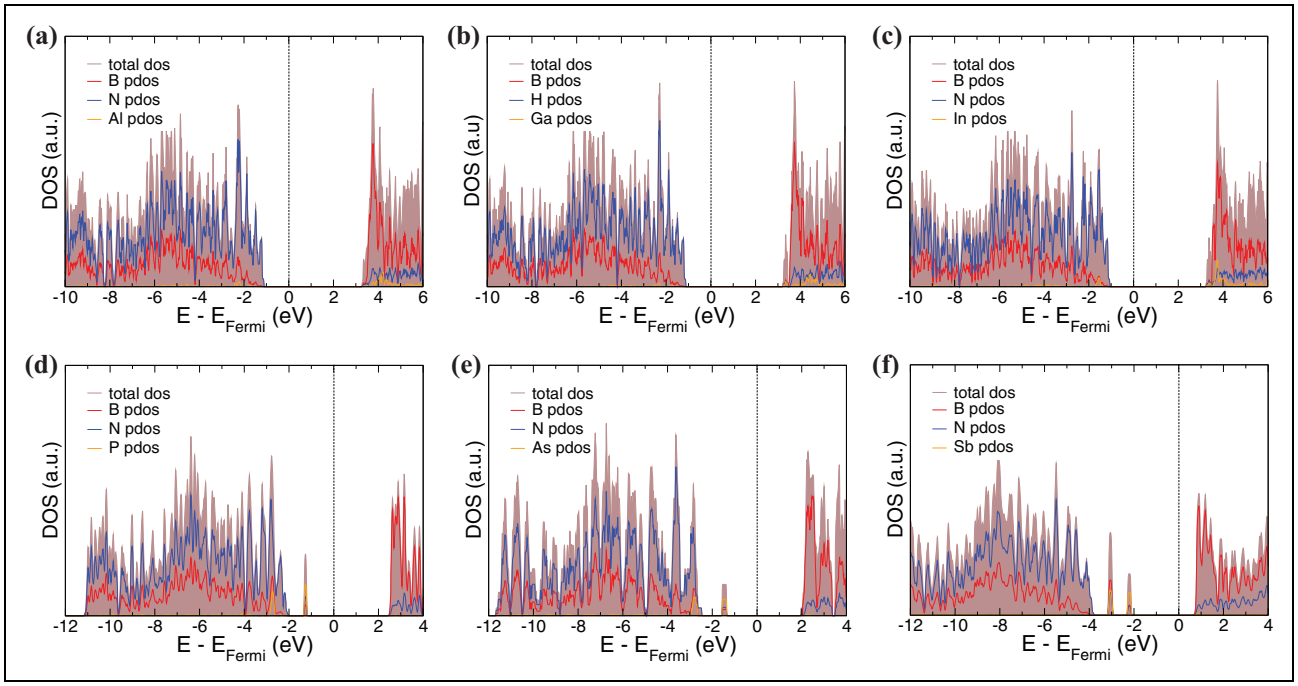

Figure 4. DOS and PDOS of B- and N-substitution in h-BN sample. DOS: density of states; PDOS: projected density of states; h-BN: hexagonal boron nitride.

state appears right below the conduction band minimum (CBm). B-substitutions, therefore, behave differently from N-substitutions in terms of electronic structure, resulting in shallow defects almost undistinguishable from the CB. This suggests that the character of the bond between the boron substitute (B_X) and the nearby nitrogen atoms is rather similar to that of B–N bonds, thus resulting in energy levels near or fused with the CB. On the contrary, the electronic structures of N-substitutions point at a different character of the bond between the nitrogen substitute (N_X) and the nearby boron atoms, resulting in the destabilization of energy levels, well distinct from the VB. A rough indicator of different bond characters can be found in the electronegativity χ. In the case of N-substitutions, the difference between the electronegativity of boron and N_X is markedly different from the electronegativity difference between boron and nitrogen, which characterizes the pristine B–N bond. In particular, while $\chi(\mathrm{N}) - \chi(\mathrm{B}) \simeq 1$, we have $\chi(\mathrm{N}_X) - \chi(\mathrm{B}) < 0.2$, which hints at a largely different bond character and energy with respect to the pristine B–N bonds. On the other hand, in the case of B-substitutions we found $1.2 < \chi(\mathrm{N}) - \chi(\mathrm{B}_X) < 1.4$, much closer to the value of pristine B–N bonds.

When considering joint substitution of two adjacent boron and nitrogen atoms and two nonadjacent boron and nitrogen atoms, we observed two occupied defect states above VBM.

The electronic structure is analyzed in Table 2. For each studied system, we report the energy of the highest occupied state (HO), E^{HO}, and of the lowest unoccupied state (LU), E^{LU}, referenced to the vacuum level, their difference $\Delta E^{\mathrm{LU,HO}} = E^{\mathrm{LU}} - E^{\mathrm{HO}}$ and the energy difference $\Delta E^{\mathrm{d}} = E_{\mathrm{defect}} - E_{\mathrm{Fermi}}$ that corresponds to the energy position of defect state (E_{defect}) with respect to the Fermi energy (E_{Fermi}). As expected, $\Delta E^{\mathrm{LU,HO}}$ values are dependent on the type of impurity considered. In case of B-substitutions, there is a decrease in $\Delta E^{\mathrm{LU,HO}}$ when moving from Al to In along the group of the periodic table. This decrease is due to the presence of an unoccupied defect state below the bottom of h-BN CB, as described above. Considering the

Table 2. Calculated energy of the HO, E^{HO}, and of the LU, E^{LU}, with respect to the vacuum level, energy difference between HO and LU, $\Delta E^{\mathrm{LU,HO}} = E^{\mathrm{LU}} - E^{\mathrm{HO}}$ and energy positions of defect states (E_{defect}) with respect to the Fermi energy (E_{Fermi}) $\Delta E^{\mathrm{d}} = E_{\mathrm{defect}} - E_{\mathrm{Fermi}}$, for the pristine h-BN and doped h-BN structures.[a]

	E^{HO} (eV)	E^{LU} (eV)	$\Delta E^{\mathrm{LU,HO}}$ (eV)	ΔE^{d} (eV)	Transition
h-BN	−4.88	−0.06	4.82	–	VBM → CBm
B_{Al}	−4.56	−0.13	4.43	–	VBM → CBm
B_{Ga}	−5.74	−1.26	4.48	3.63	VBM → LU
B_{In}	−5.69	−1.29	4.40	3.59	VBM → LU
N_P	−5.02	−1.25	3.77	−1.31	HO → CBm
N_{As}	−4.77	−1.11	3.66	−1.46	HO → CBm
N_{Sb}	−4.23	−1.17	3.06	−2.23	HO → CBm

HO: highest occupied state; LU: lowest unoccupied state; h-BN: hexagonal boron nitride; CBm: conduction band minimum; VBM: valence band maximum.

[a]In the last column, the type of electronic transition is reported. For instance, for the pristine h-BN this is the difference between CBm and VBM. For N_{As} this is the difference between CBm and the HO, while for B_{In} this is the difference between VBM and the LU.

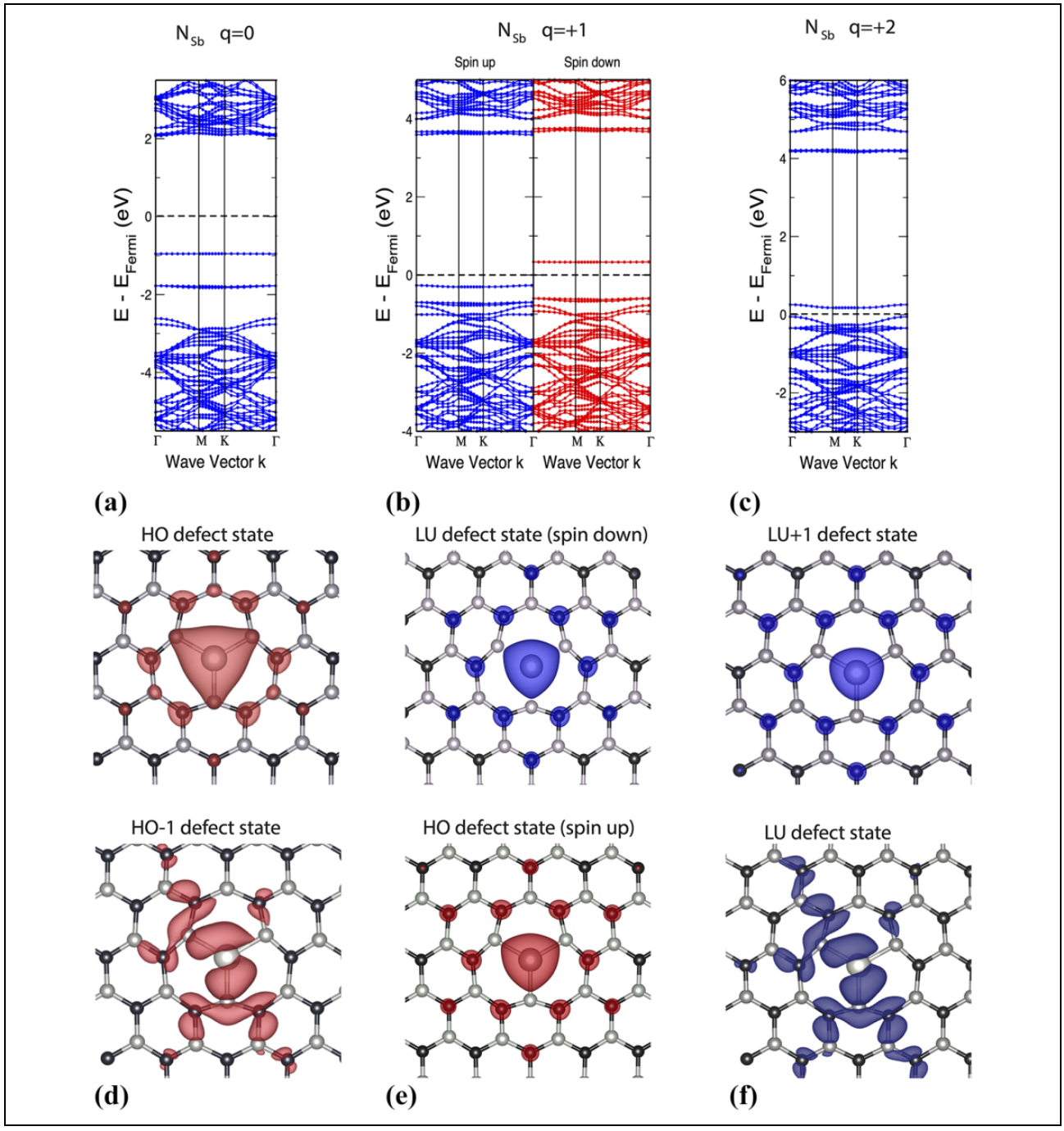

Figure 5. Electronic band structure of N_{Sb} samples with charge states $q = 0$ (a), $q = +1$ (b), and $q = +2$ (c). The corresponding electron density isosurface of charge state cases $q = 0$ (d), $q = +1$ (e), and $q = +2$ (f) of the defect states involving HO and HO-1 defect states (red isosurfaces) as well as LU and LU + 1 defect states (blue isosurfaces) are also reported. HO: highest occupied state; LU: lowest unoccupied state.

N-substitution cases, when moving from P to Sb, we observe the presence of deeper occupied defect states above the h-BN VB which corresponds to a reduction of $\Delta E^{\mathrm{LU,HO}}$.

The analysis above demonstrates that there is a strong correlation between the local anisotropic distortions and strained interatomic bonds caused by the substitutional impurities introduced in h-BN lattice, as discussed in the previous subsection, and changes in the local electronic structure. In particular, the higher the induced strain, the deeper the defect level in the semiconductor energy gap.

In addition, to understand if substitutional impurities in the h-BN matrix may give rise to defect states localized in space, we calculate the dispersion in reciprocal space and

the charge densities of the states involved in the photoexcitation process (HO-1, HO, LU, and LU+1 defect states) for neutral and charged structures. Here we report only the N_{Sb} case in Figure 5. The band structures of N_{Sb} defects at different charge states are plotted in Figure 5 (panels (a) to (c)). We set $E_{Fermi} = 0$. For the neutral state, Sb substitution introduces two defect states within the h-BN bandgap, where both defect levels are occupied (HO and HO-1). Adding further electrons to the structure leads to the filling of the nearly free-electron CBm (charge state $q = -1$ not reported here). In case of $q = +1$, the system becomes spin-polarized and its band diagram is reported in Figure 5(b). We observe the energy splitting of the original neutral HO defect state in two states with different spins located at -0.2 eV (occupied) and $+0.32$ eV (unoccupied) with respect to E_{Fermi}, respectively. When the total charge is $q = +2$, the electronic band structure undergoes a strong variation: The original HO defect state of the neutral case empties and shifts to $+0.25$ eV. In Figure 5 (panels (d) to (f)), we report the space distribution of the charge densities associated with the HO-1, HO, and LU defect states for $q = 0, +1, +2$. We have checked that the PBE functional does not artificially skew the spatial dispersion of the defect states by comparing the isosurfaces against those obtained by employing the HSE06 hybrid functional.[50] It is interesting to notice that the density is localized on the introduced impurity for all charge states.

Conclusion

We have analyzed the energetic and electronic properties of point defects in h-BN obtained through the substitution of a boron or a nitrogen atom with a heteroatom belonging to their respective group. Period by period, the computed formation energies show that B-substitutions are generally more favored than N-substitutions and both types of defects present a formation energy that increases with the period of the heteroatom. However, although energetically favored, our study of the electronic properties points out that N-substitutions do not introduce well-defined defect energy levels within the h-BN bandgap. Rather, in these cases, the defect levels tend to coalesce with the CB. On the contrary, B-substitutions appear to generate defect levels that are deep in the bandgap of h-BN. These states are occupied for neutral defects and allow for new electronic transitions between the HO defect state and CBm that can be exploited for single-photon emission.

Moreover, the study of different charge states reveals significant stability ranges for N-substitutions in the +1 charge state, in particular for N_{Sb}. The positive charge of the defect creates an empty level with fixed spin, which becomes the new LU state. This way, new transitions may take place between the new LU state and VB states with the same spin. The different energy gaps between the HO defect state and CBm in the neutral case and between VBM and the LU states for $q = +1$ seem to suggest that N-substitutions in h-BN may emit at different frequencies, depending on the charge state.

Our theoretical calculations show that the formation energies of all structures analyzed in this work are of the same order of magnitude of formation energies of substitutional oxygen at the nitrogen site and substitutional carbon at the boron site observed experimentally by means of X-ray absorption near edge structure (XANES) analysis as reported by Jungwirth et al.[31] This is evidence that substitutional impurities belonging to the 13th and 15th groups in h-BN may have equal likelihood to be observed experimentally. In addition, the deep defect levels introduced in h-BN bandgap by B-substitutions give rise to complementary emission wavelengths compared to substitutional impurities discussed in the literature.[28,31,33–35] and equally useful for different kinds of applications ranging from quantum computing to information-processing technologies.

In conclusion, our results highlight that the proposed N-substitutions in h-BN can be attractive for SPE, in particular with regard to the depth of the defect level, localization of the defect state, and the tunable emission frequency, thus serving as a fruitful starting point for future theoretical studies and possible technical applications.

Acknowledgments

The authors acknowledge the Centre for High Performance Computing (CHPC) of the Republic of South Africa for the fundamental availability of computing resources on the high-performance LENGAU cluster. The authors also wish to acknowledge the CINECA award under the ISCRA initiatives and HPC@POLITO, for the availability of high-performance computing resources.

Declaration of conflicting interests

The author(s) declared no potential conflicts of interest with respect to the research, authorship, and/or publication of this article.

Funding

The author(s) received no financial support for the research, authorship, and/or publication of this article.

ORCID iD

Francesca Risplendi https://orcid.org/0000-0002-1277-6733

References

1. Lodahl P, Mahmoodian S, and Stobbe S. Interfacing single photons and single quantum dots with photonic nanostructures. *Rev Mod Phys* 2015; 87: 347–400.
2. Aspuru-Guzik A and Walther P. Photonic quantum simulators. *Nat Phys* 2012; 8: 285–291.
3. Giovannetti V, Lloyd S, and Maccone L. Photonic quantum simulators. *Nat Photonics* 2011; 5: 222–229.
4. Lo HK, Curty M, and Tamaki K. Secure quantum key distribution. *Nat Photonics* 2014; 8: 595–604.
5. Aharonovich I, Zhou C, Stacey A, et al. Enhanced single-photon emission in the near infrared from a diamond color center. *Phys Rev B* 2009; 79: 235316.

6. Ma X, Hartmann NF, Baldwin JKS, et al. Room-temperature single-photon generation from solitary dopants of carbon nanotubes. *Nat Nanotechnol* 2015; 10: 671–675.
7. Aharonovich I and Neu E. Diamond nanophotonics. *Adv Opt Mater* 2014; 2(10): 911–928.
8. Sipahigil A, Jahnke KD, Rogers LJ, et al. Indistinguishable photons from separated silicon-vacancy centers in diamond. *Phys Rev Lett* 2014; 113: 113602.
9. Grosso G, Moon H, Lienhard B, et al. Tunable and high-purity room temperature single-photon emission from atomic defects in hexagonal boron nitride. *Nat Commun* 2017; 8: 705.
10. Dalacu D, Poole PJ, and Williams RL. Nanowire-based sources of non-classical light. *Nanotechnology* 2019; 30(23): 232001.
11. Hours J, Varoutsis S, Gallart M, et al. Single photon emission from individual GaAs quantum dots. *Appl Phys Lett* 2003; 82(14): 2206–2208.
12. Rakhlin MV, Belyaev KG, Klimko GV, et al. InAs/AlGaAs quantum dots for single-photon emission in a red spectral range. *Sci Rep* 2018; 8: 5299.
13. Sajid A, Ford MJ, and Reimers JR. Single-photon emitters in hexagonal boron nitride: a review of progress. *Rep Prog Phys* 2020; 83(4): 044501.
14. Doherty MW, Michl J, Dolde F, et al. Measuring the defect structure orientation of a single NV-centre in diamond. *New J Phys* 2014; 16(6): 063067.
15. Kubota Y, Watanabe K, Tsuda O, et al. Deep ultraviolet light-emitting hexagonal boron nitride synthesized at atmospheric pressure. *Science* 2007; 317(5840): 932–934.
16. Song L, Ci L, Lu H, et al. Large scale growth and characterization of atomic hexagonal boron nitride layers. *Nano Lett* 2010; 10(8): 3209–3215.
17. Shi Y, Liang X, Yuan B, et al. Electronic synapses made of layered two-dimensional materials. *Nat Electron* 2018; 1(8): 458–465.
18. Dabrowski J, Lippert G, Schroeder T, et al. Role of defects in the process of graphene growth on hexagonal boron nitride from atomic carbon. *Appl Phys Lett* 2014; 105(19): 191610.
19. Meric I, Dean CR, Petrone N, et al. Graphene field-effect transistors based on boron–nitride dielectrics. *Proc IEEE* 2013; 101(7): 1609–1619.
20. Cassabois G, Valvin P, and Gil B. Hexagonal boron nitride is an indirect bandgap semiconductor. *Nat Photonics* 2016; 10(4): 262–266.
21. Watanabe K, Taniguchi T, and Kanda H. Direct-bandgap properties and evidence for ultraviolet lasing of hexagonal boron nitride single crystal. *Nat Mater* 2004; 3(6): 404–409.
22. Tran TT, Bray K, Ford MJ, et al. Quantum emission from hexagonal boron nitride monolayers. *Nat Nanotechnol* 2016; 11(1): 37–41.
23. Tran TT, Zachreson C, Berhane AM, et al. Quantum emission from defects in single-crystalline hexagonal boron nitride. *Phys Rev Appl* 2016; 5: 034005.
24. Tran TT, Elbadawi C, Totonjian D, et al. Robust multicolor single photon emission from point defects in hexagonal boron nitride. *ACS Nano* 2016; 10(8): 7331–7338.
25. Koperski M, Nogajewski K, and Potemski M. Single photon emitters in boron nitride: more than a supplementary material. *Opt Commun* 2018; 411: 158–165.
26. Schell AW, Svedendahl M, and Quidant R. Quantum emitters in hexagonal boron nitride have spectrally tunable quantum efficiency. *Adv Mater* 2018; 30(14): 1704237.
27. Chejanovsky N, Rezai M, Paolucci F, et al. Structural attributes and photodynamics of visible spectrum quantum emitters in hexagonal boron nitride. *Nano Lett* 2016; 16(11): 7037–7045.
28. Bourrellier R, Meuret S, Tararan A, et al. Bright UV single photon emission at point defects in h-BN. *Nano Lett* 2016; 16(7): 4317–4321.
29. Shotan Z, Jayakumar H, Considine CR, et al. Photoinduced modification of single-photon emitters in hexagonal boron nitride. *ACS Photonics* 2016; 3(12): 2490–2496.
30. Jungwirth NR, Calderon B, Ji Y, et al. Temperature dependence of wavelength selectable zero-phonon emission from single defects in hexagonal boron nitride. *Nano Lett* 2016; 16(10): 6052–6057.
31. McDougall NL, Partridge JG, Nicholls RJ, et al. Influence of point defects on the near edge structure of hexagonal boron nitride. *Phys Rev B* 2017; 96: 144106.
32. Katzir A, Suss JT, Zunger A, et al. Point defects in hexagonal boron nitride. I. EPR, thermoluminescence, and thermally-stimulated-current measurements. *Phys Rev B* 1975; 11: 2370–2377.
33. Taniguchi T and Watanabe K. Synthesis of high-purity boron nitride single crystals under high pressure by using Ba–BN solvent. *J Cryst Growth* 2007; 303(2): 525–529.
34. Du XZ, Li J, Lin JY, et al. The origin of deep-level impurity transitions in hexagonal boron nitride. *Appl Phys Lett* 2015; 106(2): 021110.
35. Museur L, Anglos D, Petitet JP, et al. Photoluminescence of hexagonal boron nitride: effect of surface oxidation under UV-laser irradiation. *J Lumin* 2007; 127(2): 595–600.
36. Greenwood NN and Earnshaw AE. *Chemistry of the elements*. 2nd ed. Oxford: Butterworth-Heinemann, 1997.
37. Giannozzi P, Baroni S, Bonini N, et al. Quantum ESPRESSO: a modular and open-source software project for quantum simulations of materials. *J Phys Condens Matter* 2009; 21(39): 395502.
38. Giannozzi P, Andreussi O, Brumme T, et al. Advanced capabilities for materials modelling with Quantum ESPRESSO. *J Phys Condens Matter* 2017; 29(46): 465901.
39. Schlipf M and Gygi F. Optimization algorithm for the generation of ONCV pseudopotentials. *Comput Phys Commun* 2015; 196: 36–44.
40. Perdew JP, Burke K, and Wang Y. Generalized gradient approximation for the exchange-correlation hole of a many-electron system. *Phys Rev B* 1996; 54: 16533–16539.
41. Monkhorst HJ and Pack JD. Special points for Brillouin-zone integrations. *Phys Rev B* 1976; 13: 5188–5192.
42. Zobelli A, Ewels CP, Gloter A, et al. Vacancy migration in hexagonal boron nitride. *Phys Rev B* 2007; 75: 094104.

43. Komsa HP, Rantala TT, and Pasquarello A. Finite-size supercell correction schemes for charged defect calculations. *Phys Rev B* 2012; 86: 045112.
44. Zhang SB and Northrup JE. Chemical potential dependence of defect formation energies in GaAs: application to Ga self-diffusion. *Phys Rev Lett* 1991; 67: 2339–2342.
45. Komsa HP, Berseneva N, Krasheninnikov AV, et al. Charged point defects in the flatland: accurate formation energy calculations in two-dimensional materials. *Phys Rev X* 2014; 4: 031044.
46. Van de Walle CG and Neugebauer J. First-principles calculations for defects and impurities: applications to III-nitrides. *J Appl Phys* 2004; 95(8): 3851–3879.
47. Freysoldt C, Grabowski B, Hickel T, et al. First-principles calculations for point defects in solids. *Rev Mod Phys* 2014; 86: 253–305.
48. Freysoldt C, Neugebauer J, and Van de Walle CG. Fully *ab initio* finite-size corrections for charged-defect supercell calculations. *Phys Rev Lett* 2009; 102: 016402.
49. Huang B and Lee H. Defect and impurity properties of hexagonal boron nitride: a first-principles calculation. *Phys Rev B* 2012; 86: 245406.
50. Heyd J, Scuseria GE, and Ernzerhof M. Hybrid functionals based on a screened Coulomb potential. *J Chem Phys* 2003; 118(18): 8207–8215.